Combustion and Emission Characterization of n –Butanol Fueled HCCI Engine

Article *in* Journal of Energy Resources Technology, Transactions of the ASME · July 2014

DOI: 10.1115/1.4027898

2 authors, including:

Avinash Kumar Agarwal
Indian Institute of Technology Kanpur
580 PUBLICATIONS **23,048** CITATIONS

Combustion and Emission Characterization of *n*-Butanol Fueled HCCI Engine

Rakesh Kumar Maurya[1]
Engine Research Laboratory,
Department of Mechanical Engineering,
Indian Institute of Technology Kanpur,
Kanpur 208016, India

Avinash Kumar Agarwal[2]
Engine Research Laboratory,
Department of Mechanical Engineering,
Indian Institute of Technology Kanpur,
Kanpur 208016, India
e-mail: akag@iitk.ac.in

Biofuels are attracting global attention as alternate transportation fuels due to advantages of their being produced from locally available renewable resources, lower pollution potential, and biodegradable nature. Butanol is fast emerging as one of the competitive biofuels for use in transportation engines. Homogeneous charge compression ignition (HCCI) engines have shown great potential for higher engine efficiency and ultralow NO_x and particulate matter (PM) emissions. This experimental study is therefore carried out to combine the advantages of biofuels and HCCI engines, both. Detailed performance, combustion, and emission characteristics of n-butanol fueled HCCI engine are investigated experimentally. The study is conducted on a four cylinder diesel engine, whose one cylinder was modified to operate in HCCI combustion mode. Port fuel injection technique was used for homogeneous charge preparation in the intake manifold. Auto-ignition of fuel in the engine cylinder was achieved by intake air preheating. In-cylinder pressure-crank angle data acquisition with subsequent heat release analyses and exhaust emission measurements were done for combustion and emission characterization. In this paper, the effect of intake air temperature and air–fuel ratio on the combustion parameters, thermal and combustion efficiency, ringing intensity (RI), and emissions from n-butanol fueled HCCI engine were analyzed and discussed comprehensively. Empirical correlations were derived to fit the experimental data for various combustion parameters. [DOI: 10.1115/1.4027898]

Keywords: HCCI, n-butanol, rate of heat release, combustion efficiency, ringing intensity, emissions

1 Introduction

In the current scenario, biofuels are drawing attention of researcher globally due to various factors such as energy security and diversity, uncertainty regarding crude oil prices, and harmful environmental impact of emissions from combustion of fossil fuels. In the automotive sector, several biofuels are employed globally such as biodiesel, methanol, and ethanol. All these biofuels can be obtained from renewable resources in contrast to fossil fuels (gasoline and diesel), which are exploited from earth's subsurface. Biodiesel and alcohols are widely used biofuels in internal combustion (IC) engines [1]. Among alcohols, ethanol is considered as the primarily alternative fuel for IC engine applications globally. Methanol is also used as an alternate fuel in IC engines, but to a much lesser extent [1,2]. Methanol is mainly obtained from coal or petroleum, while ethanol is biomass-based renewable fuel, produced mainly from sugar forms [1–4]. Therefore, ethanol is considered superior to methanol due to its origin from renewable resource. Ethanol is widely used as a fuel additive and as an alternative fuel in many countries [1]. However, ethanol is a hygroscopic alcohol, which absorbs moisture, when exposed to atmospheric air. On the other hand, *n*-butanol offers almost same advantages, as offered by ethanol with an additional benefit of nonhygroscopic nature. Butanol is therefore a competitive biofuel for utilization in IC engines. Butanol is also a renewable fuel, which can be produced by alcoholic fermentation of the biomass feedstock [1,5,6].

Two main challenges faced by automotive industry are (i) improving fuel economy and (ii) reducing exhaust emissions. Two conventional combustion modes used in IC engines are spark ignition (SI) and compression ignition (CI). To meet current and future stringent emission norms, exhaust gas after-treatment devices are deployed. To reduce the cost of after-treatment devices, alternative combustion technologies for in-cylinder emission reduction are proposed. HCCI combustion mode is the third alternative combustion mode for the IC engines. HCCI mode has great potential for higher thermal efficiencies and ultralow NO_x and PM emissions. HCCI combustion concept has already been demonstrated successfully on various alternative fuels such as alcohols, CNG, DME, and LPG, as well as conventional gasoline and diesel fuels [7–16]. Fuel flexibility features of HCCI engine could alleviate dependence on fossil fuels by enabling the use of various alternative fuels [17]. Butanol is one such alternate biofuel for IC engines and is used in SI engines [18–22] and diesel engines [23–26] in blended or pure form. Butanol has higher heating value compared to ethanol or methanol.

Gu et al. conducted experimental investigations of emissions using gasoline–butanol blends with exhaust gas recirculation in a SI engine [27]. They found that butanol has lower brake specific NO_x emissions but higher brake specific HC and carbon monoxide (CO) emissions. Chotwichien et al. found that butanol–diesel blend was more suitable to CI engines due to higher solubility of butanol in mineral diesel compared to ethanol [28]. Constant volume combustion chamber studies conducted by Liu et al. using pure butanol and biodiesel showed that butanol is more suitable to diesel engines in terms of its combustion characteristics [29]. However, very limited studies are conducted for utilization of *n*-butanol in low temperature combustion engines [30] and HCCI engine. This motivated the researchers to use *n*-butanol as a fuel in HCCI engine. In this study, performance, combustion, and emission characteristics of *n*-butanol in HCCI engine is

[1]Present address: School of Mechanical Materials and Energy Engineering, Indian Institute of Technology Ropar, Rupnagar 140001, India.
[2]Corresponding author.

Contributed by the Internal Combustion Engine Division of ASME for publication in the JOURNAL OF ENERGY RESOURCES TECHNOLOGY. Manuscript received November 11, 2013; final manuscript received June 19, 2014; published online July 29, 2014. Editor: Hameed Metghalchi.

investigated and compared with characteristics of baseline fuel "gasoline" in the same engine operating under similar conditions. In Secs. 2 and 3, experimental setup used for this study is described and then the results of experiments performed for combustion, emission, and combustion characteristics of *n*-butanol are presented. Finally, conclusions from this study are outlined.

2 Experimental Setup

Our previous work [31,32] covers detailed explanation of the experimental setup; therefore, in this section, only brief description of the engine setup and experimental procedure is given. A four cylinder diesel engine was modified and HCCI combustion was achieved in one of the four cylinders. Experimental observations for this study are made on this HCCI cylinder only. The technical specifications of the unmodified test engine are provided in Table 1.

Schematic of the experimental setup is shown in Fig. 1. Intake, exhaust, and fuel systems of HCCI cylinder are separated from the other three cylinders and are therefore independent. The engine was coupled with an eddy current dynamometer. Test fuels used for the present investigation are *n*-butanol and baseline gasoline. Port fuel injection was used for homogeneous charge preparation in the intake manifold. The fuel was injected in the intake manifold, where fuel vaporizes and mixes with preheated intake air. Intake air was preheated using electrical heater to achieve auto-ignition of the combustible mixture in the cylinder. Fuel injection timing and fuel quantity were controlled using a microcontroller (cRIO: compact reconfigurable input-output, NI) and a customized injection driver circuit. A hot-film air mass flow meter was installed in the intake manifold for measurement of actual air mass delivered to the HCCI cylinder. Exhaust gas emissions were measured using raw exhaust gas emission analyzer (EXSA1500, Horiba). Crank angle position was measured by a precision optical shaft encoder (H25D-SS-2160-ABZC, BEI) mounted on the engine crankshaft, which has resolution of a 1/6 of a crank angle degree.

In-cylinder pressure was measured by piezoelectric pressure transducer, mounted flush with the cylinder head. A LabVIEW based program was used for in-cylinder pressure data acquisition and data processing for heat release and combustion parameter calculations. In-cylinder pressure data for 2000 consecutive engine cycles were recorded for each engine test conditions. Combustion parameters were calculated from the rate of heat release (RoHR) curve. In this study, RoHR was calculated using the following equation.

Rate of heat release (RoHR): RoHR is calculated by zero dimensional heat release model from measured in-cylinder pressure [33]. RoHR was calculated as

$$\frac{\partial Q}{\partial \theta} = \frac{\gamma}{\gamma - 1} p \frac{dV}{d\theta} + \frac{1}{\gamma - 1} V \frac{\partial p}{\partial \theta} + \frac{\partial Q_w}{\partial \theta} + \frac{\partial Q_{\text{crevice}}}{\partial \theta} \tag{1}$$

In these calculations, heat loss through crevices is assumed to be small and is therefore neglected.

The ratio of specific heats used in the above equation is calculated by the following equation [34]:

Table 1 Test engine specifications

Make/Model	Mahindra/Loadking
No. of cylinders	Four
Displaced volume	652 cc/cylinder
Stroke/Bore	94/94 mm
Connecting rod length	158 mm
Compression ratio	17.5:1
Number of valves	2/cylinder
Exhaust valve open/close	56 deg BBDC/5 deg ATDC
Inlet valve open/close	10 deg BTDC/18 deg ABDC

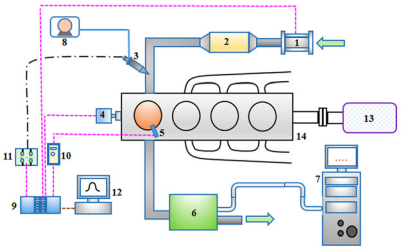

Fig. 1 Schematic of the experimental setup

$$\gamma = \gamma_0 - \frac{k}{100}\frac{T}{1000} \tag{2}$$

γ_0 is the γ value at some reference temperature, usually 300 K. γ_0 is dependent on the gas composition. For atmospheric air, γ_0 is 1.4 and for lean air/fuel mixtures 1.38 is a usable value. The constant k is usually set at 8.

Rate of heat loss through the combustion chamber walls is calculated using the following equation:

$$\frac{\partial Q_w}{\partial \theta} = \frac{h(T - T_w)A}{360N} \quad [\text{J/CAD}] \tag{3}$$

Here, h is heat transfer coefficient, T_w is the average cylinder wall temperature, A is the actual cylinder wall area, and N is the engine speed. It is normally assumed that T_w is constant over the entire engine cycle. h, T, and A are functions of crank angle position. In this study, heat transfer coefficient is calculated by Hohenberg Model given by the following equation [35]:

$$h = \alpha_s V^{-0.06} P^{0.8} T^{-0.4} \left(S_p + 1.4\right)^{0.8} \tag{4}$$

Here, S_p is the mean piston speed, α_s is scaling factor, P, V, and T are pressure, volume, and temperature of the combustion chamber, respectively. Soyhan et al. found that the Hohenberg heat transfer model, which has no explicit combustion compression velocity term, gives better agreement with their experiments [35]. Scaling factor is determined by tuning procedure given in Ref. [32].

Ringing Intensity (RI): For assessment of combustion noise from the HCCI engines, "Ringing Intensity" is calculated using the following equation [36]:

$$\text{RI} = \frac{\sqrt{\gamma R T_{\max}}}{2\gamma P_{\max}} \left[\beta \left(\frac{dP}{dt}\right)_{\max}\right]^2 \tag{5}$$

where $(dP/dt)_{\max}$ is the maximum pressure rise rate, $P_{\max}$ is the peak in-cylinder pressure, and $T_{\max}$ is the maximum of mass averaged in-cylinder temperature (calculated using ideal gas law). γ is the ratio of specific heats (C_p/C_v) and R is the gas constant. β is a tuning parameter, which relates the amplitude of pressure pulsations to the maximum pressure rise rate, and is set to 0.05 here.

Gross indicated thermal efficiency is defined as the ratio between the work on the piston during the compression and expansion stroke ($W_{ind,g}$) to the input fuel energy [37].

$$\eta_{i,g} = \frac{W_{ind,g}}{m_f q_{LHV}} \tag{6}$$

Here, m_f is fuel mass injected per cycle and q_{LHV} is the lower heating value of the fuel.

Combustion efficiency (η_{com}) is calculated from the following equation [38]:

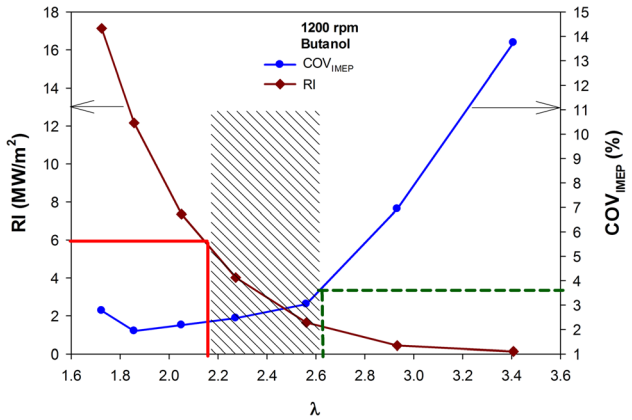

Fig. 2 Illustration of method for determination of HCCI operating range

$$\eta_{com} = \frac{\sum \text{ROHR}}{Q_{in}} \times 100 \tag{7}$$

Here, $\sum$ROHR is the integrated heat release rate; Q_{in} is total heat content of the introduced fuel.

Coefficient of variation (COV) of indicated mean effective pressure (IMEP) is calculated using the following equation:

$$\text{COV of IMEP} = \frac{\sigma_{IMEP}}{\overline{IMEP}} \times 100 \tag{8}$$

Here, $\overline{IMEP} = \sum_{i=1}^{N}(IMEP_i/N)$; i is the sample of interest and N is the number of samples.

Standard deviation (σ) of IMEP quantifies how widely IMEP values are dispersed from the mean and calculated by the following equations:

$$\text{STD of IMEP } (\sigma_{IMEP}) = \sqrt{\frac{1}{N-1}\sum_{i=1}^{N}(IMEP_i - \overline{IMEP})} \tag{9}$$

3 Results and Discussion

In this section, the experimental results are presented for gasoline and *n*-butanol fueled HCCI combustion at different engine operating conditions of varying intake air temperature and air–fuel ratio at different engine speeds. Performance, emissions, and combustion characteristics are analyzed in Secs. 3.1 to 3.6.

3.1 HCCI Operating Range Determination. A suitable criterion for stable HCCI operating range is required for the HCCI engine combustion studies because it lacks any direct control on the ignition timings. HCCI operating range is defined by considering operational limitations due to combustion noise, combustion stability, peak in-cylinder pressure, and emission levels. Size and shape of the HCCI operating range depends on the method used to achieve HCCI combustion. In this study, intake air preheating was used to attain the HCCI combustion. The HCCI operating region with intake air preheating was determined by high and low load limits referred as knock and misfire limits, respectively. In this study, RI has been used as a criterion to define high load limit. Acceptable RI value used in this study is less than 6 MW/m^2. This value is taken from the published literature for similar displacement engines [39,40].

Figure 2 illustrates determination of HCCI operating range. RI values increase with decrease in λ (richer mixture) and maximum limit of RI (6 MW/m^2) and corresponding λ values is shown. For a mixture richer than this, λ value does not fall in acceptable HCCI operating range. At low loads, fuel flow rate decreases (higher λ), therefore, HCCI combustion rate decreases and combustion phasing is retarded, which leads to reduction in-cylinder pressure and temperature. Auto-ignition is dependent on in-cylinder pressure and temperature, in order to initiate the chemical reactions; therefore, with late combustion phasing, cycle-to-cycle variations increase. There is a risk of misfire with too late combustion phasing. Reduction in average combustion temperature also results in higher unburned charge, characterized by high CO and THC emissions. Fluctuations of IMEP can be used as a measure of cycle-to-cycle variations and expressed as COV_{IMEP} (defined in the experimental setup section). The COV of IMEP is calculated by using data of 2000 consecutive engine cycles and was used to define the low load HCCI limit (misfire limit). Acceptable COV_{IMEP} value used in this study is less than 3.5% (value taken from literature [39,40] for similar displacement engine).

It can be observed from Fig. 2 that COV_{IMEP} value increases with increase in λ (i.e., for leaner mixture). Maximum limit of COV_{IMEP} and corresponding λ value are illustrated in Fig. 2. Mixtures leaner than this λ value are not in acceptable HCCI operating range. Hence, λ values in shaded region are defined as acceptable HCCI operating range.

Figures 3 and 4 show HCCI operating range using above criterion of high and low load limits for gasoline, and *n*-butanol, respectively, at engine speeds of 1200 rpm and 2400 rpm. In Figs. 3 and 4, contour lines represent constant IMEP lines. Parameters presented by contour lines are mentioned on each graph.

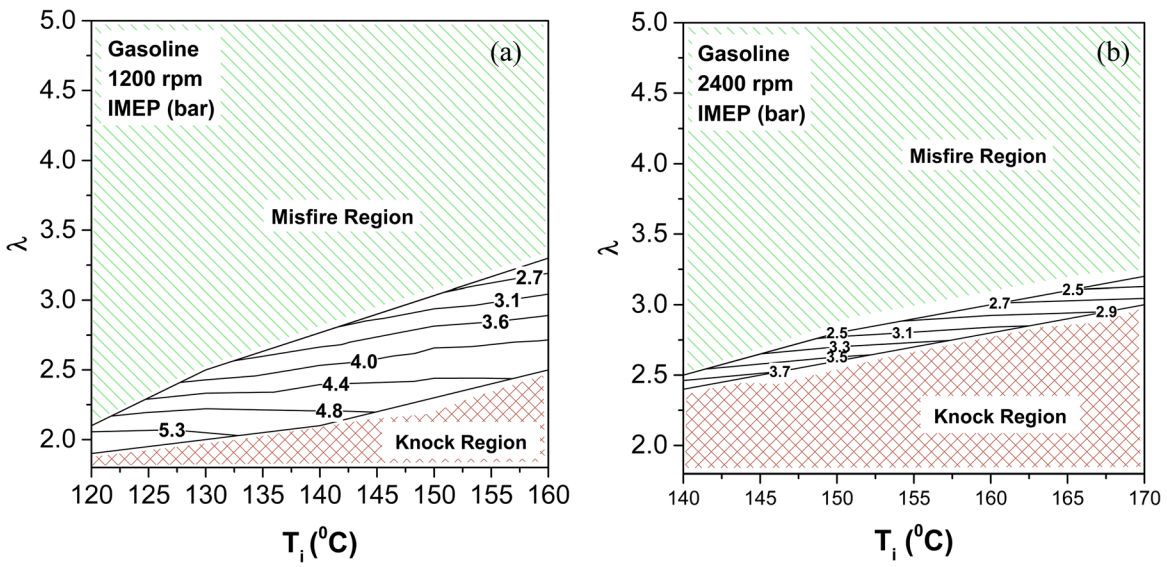

Fig. 3 HCCI operating range for gasoline at (*a*) 1200 rpm (*b*) 2400 rpm

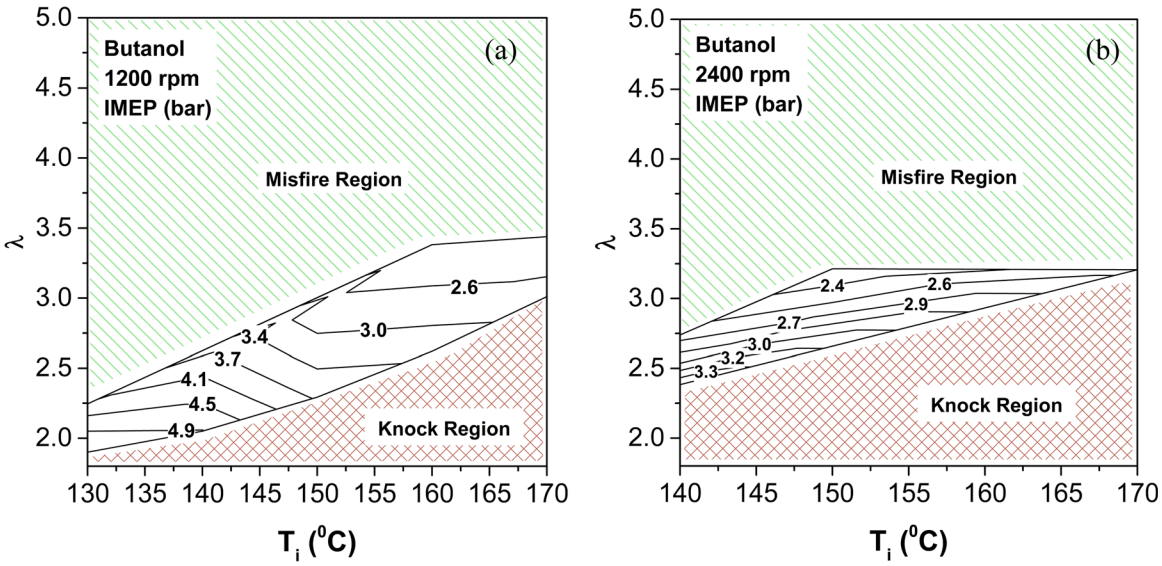

Fig. 4 HCCI operating range for *n*-butanol at (*a*) 1200 rpm (*b*) 2400 rpm

It can be observed from Fig. 3 that IMEP contours are more horizontally inclined for both test fuels at both speeds. This observation indicates that IMEP (contour lines) is largely affected by λ in the HCCI operating region. Intake air temperature affects mainly combustion phasing, which has a weak effect on IMEP in HCCI operating region, defined by high and low load limit discussed above. It is obvious that the engine output in the HCCI operating range is determined by λ since the richer mixture (higher energy input) leads to higher engine output. It can be noticed from Figs. 3 and 4 that IMEP decreases as engine operates on leaner mixture, and IMEP increases as engine operating point moves closer to richer mixture and lower intake air temperatures.

It is also observed from Figs. 3 and 4 that operating region's area decreases with increasing engine speed for both test fuels. As the engine speed increases, minimum λ (richest mixture) in HCCI operating range increases (i.e., mixture becomes leaner) for both fuels. Therefore, higher load boundary decreases, as the engine speed increases due to lower energy input (leaner mixture). Higher engine speed requires higher intake air temperature for auto-ignition of the mixture (Figs. 3 and 4). Higher intake air temperature is required for two reasons. The auto-ignition temperature is dependent on the pressure and temperature history. First, there is less time for chemical reactions to setoff the auto-ignition at higher engine speeds. The other reason is more engine specific. Due to small inlet valve diameter and pressure drop over the intake heater, volumetric efficiency of the engine decreases with increased engine speed. To compensate for this pressure drop, the intake air temperature has to be raised at higher engine speed. However, higher engine speed reduces the heat transfer, which inturn increases combustion chamber temperature. This is an opposing factor, which lowers the requirement of higher intake air temperature. Therefore, requirement of higher intake air temperature depends upon the dominating factor between the two opposing factors given above.

3.2 IMEP Variation Analysis. Engine load can be expressed as torque or MEP. For comparing engines of different sizes, MEP is preferred [33]. Engine operating ranges (in terms of IMEP) for gasoline and *n*-butanol fuels are shown in Fig. 5. Maximum and minimum values of IMEP were evaluated by applying the criterion for knocking and misfire limits, respectively. It can be noticed from Fig. 5 that HCCI operating range of *n*-butanol was slightly smaller than gasoline. Maximum IMEP was 5.6 and 5.2 bar at 1200 rpm for gasoline and *n*-butanol. At higher engine speed, IMEP was lower due to leaner mixture operation in order to avoid ringing.

It can be observed from the above subsection that IMEP in HCCI operating range mainly depends on λ. IMEP versus λ and fuel energy were plotted (Fig. 6) to further understand the characteristics of IMEP variation at all test conditions (including the test points outside HCCI operating range). It can be noticed that richer mixtures have higher IMEP.

It can be noticed from Fig. 6(*a*) that IMEP has a direct correlation with λ and this correlation appears to be linear ($R^2 = 0.81$) with only a few conditions outside the 95% prediction band. Figure 6(*b*) shows the correlation of IMEP with fuel energy input during combustion cycle using *n*-butanol for all test points at 1200, 1800, and 2400 rpm. It can be noticed that the correlation with fuel energy per cycle ($R^2 = 0.90$) was better than correlation with λ ($R^2 = 0.81$). This suggests that IMEP depends more on fuel energy injection per cycle compared to λ.

To provide a clear understanding of the variation of IMEP, all experimental data collected at 1200 and 2400 rpm for gasoline (70 data points) and *n*-butanol (63 data points) were used to find the empirical correlations. Parameters selected to characterize the IMEP variations are energy input per cycle (J/cycle) (magnitude parameter), P_{max} (bar) (magnitude parameter), and CAP_{max} (CAD aTDC) (location parameter). The correlation found to work well for the experimental data is

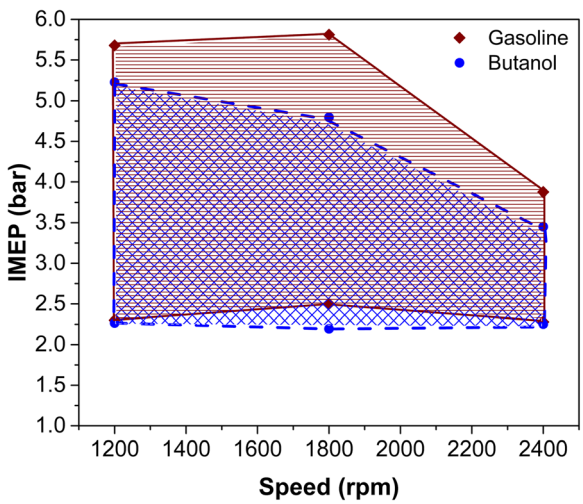

Fig. 5 Comparison of HCCI operating range for gasoline and *n*-butanol

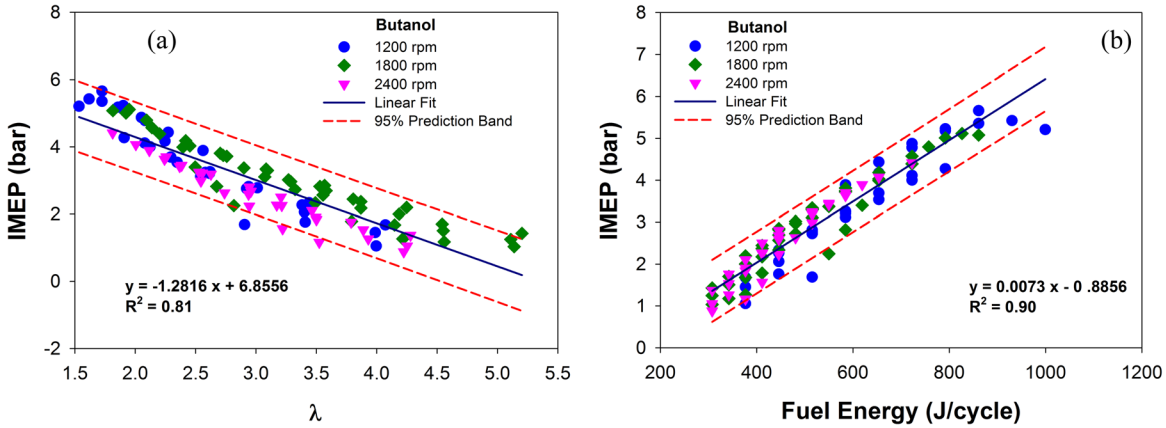

Fig. 6 Variation of IMEP with (*a*) λ (*b*) fuel energy per cycle for *n*-butanol HCCI

Table 2 Empirical constants and coefficient of determination for IMEP calculation

Fuel	*a*	*b*	*c*	*d*	R^2
Gasoline	−2.5541	0.0052	0.0499	0.0863	0.9735
n-Butanol	−3.6957	0.0039	0.0644	0.1276	0.9589

$$\text{IMEP} = a + b(\text{Energy}) + c(P_{\max}) + d(\text{CAP}_{\max})$$

Here, a, b, c, and d are constant, which are determined using regression of experimental data. Empirical correlation found have good coefficient of determination ($R^2 > 0.95$). Values of constants and coefficient of determination found during the regression analysis of experimental data are given in Table 2.

Correlations found for gasoline and *n*-butanol were used to predict the IMEP at 1800 rpm. Predicted values of IMEP were compared with experimental values (not used to derive empirical correlation) shown in Fig. 7. The results indicated that the simple correlations capture the trend of IMEP variations and presents good agreement with the experimental data for majority of engine operating conditions. An uncertainty of 0.3 bar was found in the predictions using these correlations. The uncertainty was evaluated by 2σ, where σ was the standard deviation of the residual error between predicted and experimental values. This meant that the true value with 95% confidence lie within 2σ of the estimated value [41]. This correlation suggested that the main parameters affecting the engine load (IMEP) in the HCCI engine were fuel energy injected per cycle, peak cylinder pressure, and crank angle position corresponding to peak cylinder pressure.

3.3 Combustion Efficiency Analysis. Combustion efficiency is a parameter which represents how well the engine burns the fuel. In this study, the combustion efficiency was calculated as the ratio of total heat release to total energy supplied (equations given in Sec. 2). Figure 8 shows the variation of combustion efficiency with relative air–fuel ratio using gasoline and *n*-butanol at different intake air temperatures for all test points (including knock and misfire range). With reasonably rich mixtures, combustion efficiency was high. At leaner mixtures, the limit for stable combustion after auto-ignition was reached. Very small heat released from the combustion resulted in severe quenching [42].

Combustion efficiency was higher for richer mixture (lower λ) as well as for higher inlet charge temperatures. This was because richer mixture and higher inlet charge temperature increase overall in-cylinder temperature, and consequently, expedite the burning rates. Additionally, CA_{50} is advanced for higher in-cylinder temperatures, and a more complete fuel oxidation is possible before the piston expansion reduces temperatures to a level, which is too low for oxidation reactions to complete. If more fuel is burnt, more thermal energy will be available to be transformed into mechanical work, and the indicated efficiency would also become higher.

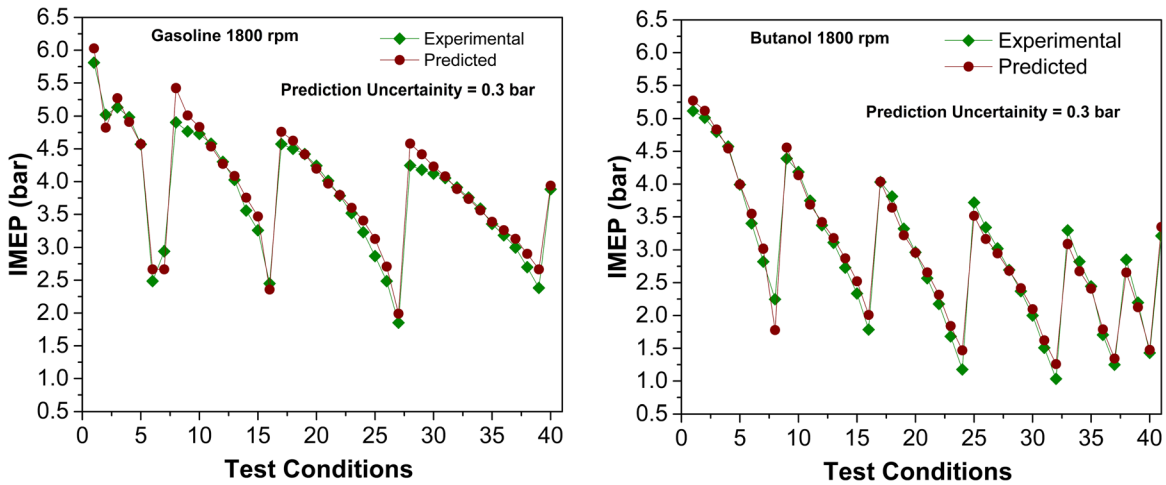

Fig. 7 Comparison of predicted and experimental IMEP for gasoline and *n*-butanol HCCI

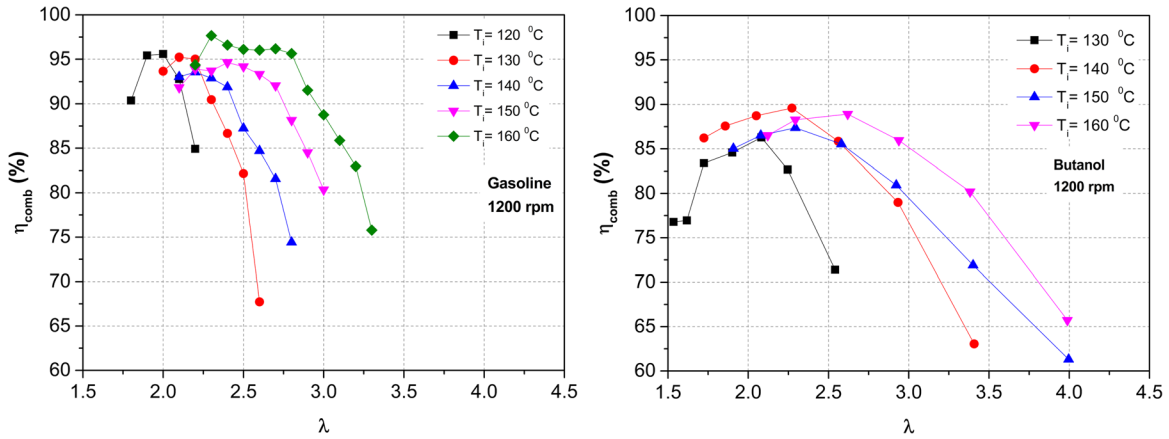

Fig. 8 Effect of λ on combustion efficiency for gasoline and *n*-butanol HCCI at different intake air temperatures

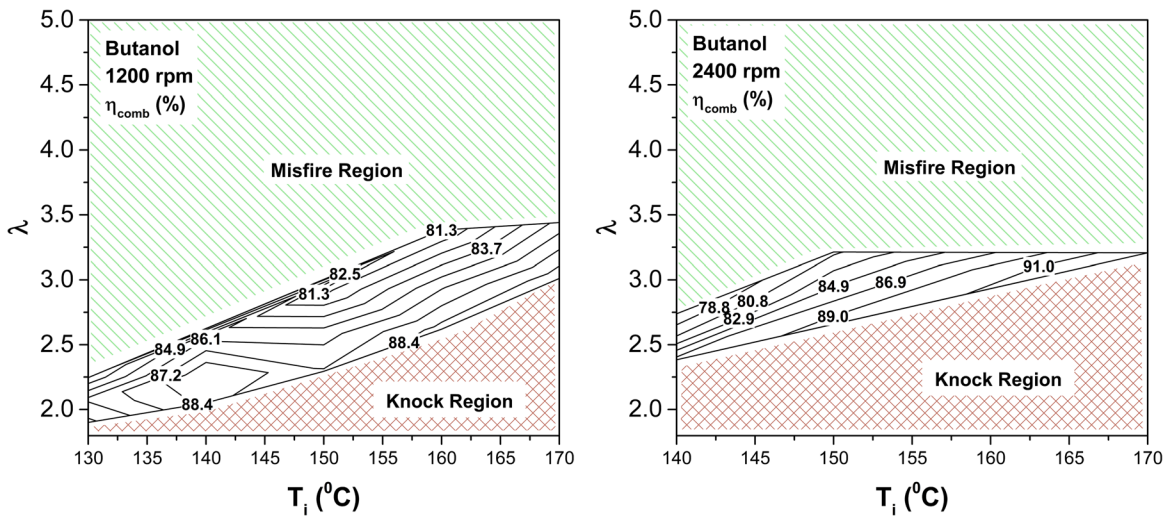

Fig. 9 Variation of combustion efficiency in HCCI operating range for *n*-butanol

In very advanced combustion phasing, rate of pressure rise increases drastically and engine knocking starts. During knocking in the engine (with very rich mixture and high inlet charge temperature), combustion efficiency decreases (Fig. 8). Combustion efficiency in gasoline was up to 96% and *n*-butanol showed relatively lower combustion efficiency up to 90% (Fig. 8). Boiling point and heat of vaporization of *n*-butanol were higher as compared to gasoline. *n*-Butanol has relatively inferior evaporation and mixing characteristics, which might be the reason for relatively lower combustion efficiency observed for *n*-butanol.

Figure 9 shows the variation of combustion efficiency in HCCI operating range for *n*-butanol at 1200 and 2400 rpm. It can be observed that combustion efficiency is higher for richer mixtures and higher inlet air temperatures, as explained earlier. Combustion efficiency was highest, close to knock boundary and lowest, close to misfire boundary, for both fuels. Contour lines of constant combustion efficiency are inclined, indicating the dependency of combustion efficiency on intake air temperature and λ.

3.4 Indicated Thermal Efficiency Analysis. The gross indicated efficiency was computed using measured fuel flow and calculated IMEP during the compression and expansion strokes. HCCI combustion concept has high thermal efficiency, and for a given compression ratio, the indicated efficiency was mainly dependent on the combustion efficiency and combustion phasing [43]. In the HCCI engine, heat losses were expected to be relatively lower compared to conventional CI or SI engine due to lower combustion temperatures and shorter combustion duration. Additionally, HCCI engine operates on the homogeneous fuel–air mixture, which does not generate soot during combustion; therefore, radiation losses are also not present.

Figure 10 shows the gross indicated thermal efficiency for HCCI using different intake air temperatures (T_i) for gasoline and *n*-butanol at 1200 rpm. It can be noticed from the figure that at each intake air temperature, indicated thermal efficiency is lower for leaner mixtures due to retarded combustion phasing and it increases as the combustible mixtures becomes richer. This trend was found for both fuels at each intake air temperature. It is also observed that the best efficiency is observed for low intake air temperatures and a fairly rich mixture. With leaner mixtures, the efficiency drops significantly at lower intake air temperatures due to late combustion phasing. At the highest intake air temperature, indicated thermal efficiency is lower for relatively richer mixtures and it declines further, when mixtures become too lean. It can also be noticed from Fig. 10 that *n*-butanol has lower indicated thermal efficiency as compared to gasoline due to its lower combustion efficiency (Fig. 8).

Indicated specific fuel consumption (ISFC) is the ratio of fuel consumed to the indicated power produced by the engine.

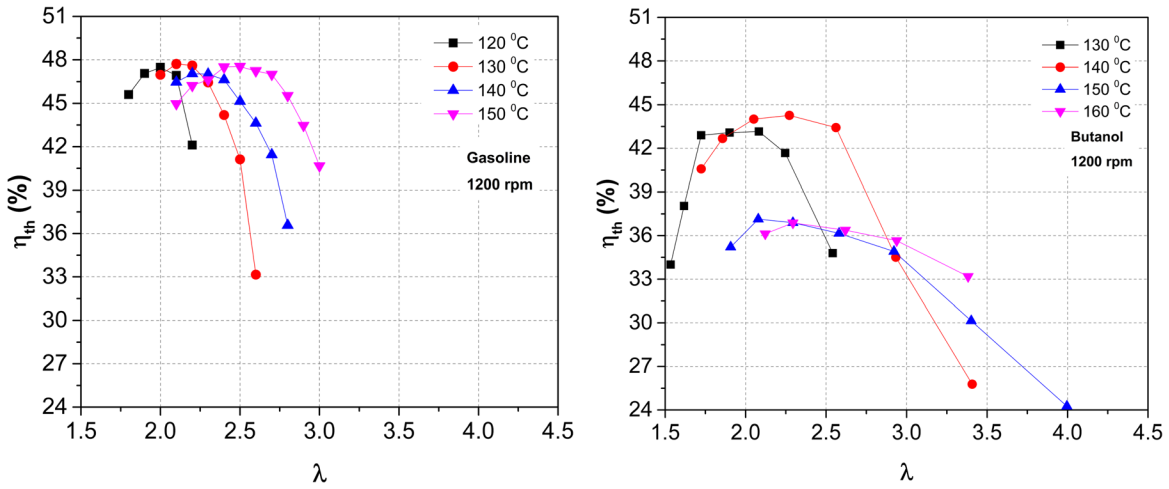

Fig. 10 Effect of λ and T_i on gross indicated thermal efficiency of gasoline and *n*-butanol HCCI

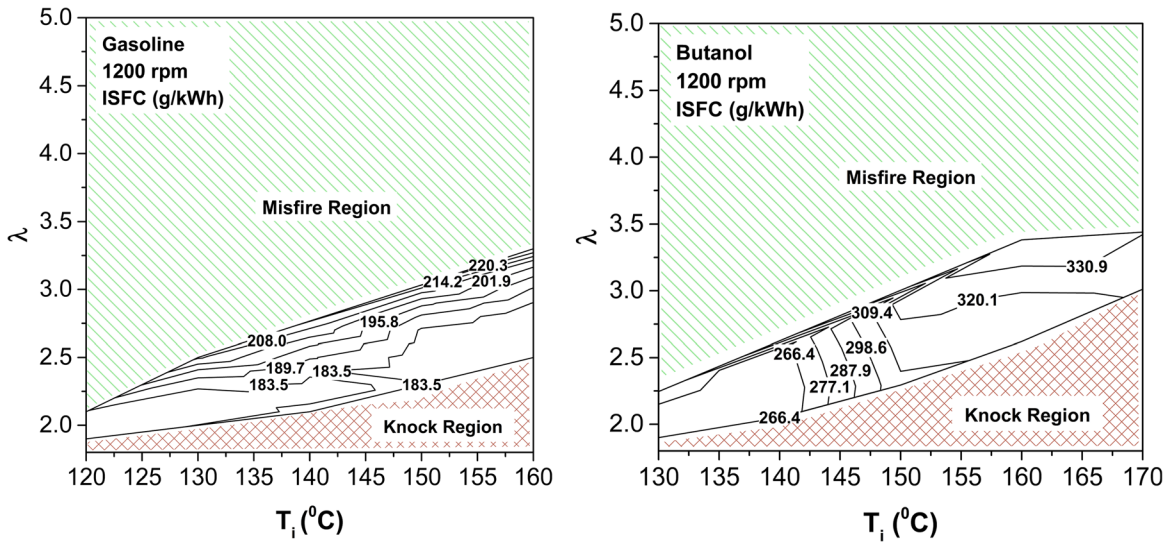

Fig. 11 Variation of ISFC in HCCI operating range for gasoline and *n*-butanol

The indicated power is calculated from the pressure–volume curve. ISFC has inverse relationship with the indicated thermal efficiency; therefore, the maximum indicated efficiency corresponds to the minimum ISFC. Figure 11 shows the variation of ISFC in HCCI operating range for gasoline and *n*-butanol.

It can be noticed from Fig. 11 that near misfire boundary and higher intake air temperature, ISFC was higher due to lower indicated thermal efficiency. Closer to the knock boundary, ISFC was relatively lower for both fuels. It can also be noticed that ISFC for *n*-butanol was higher as compared to gasoline due to lower indicated thermal efficiency and calorific value of *n*-butanol.

3.5 Ringing Intensity Analysis. The HCCI combustion mode is similar to the knock phenomenon in SI engines because of nearly simultaneous self-ignition at multiple points in the combustion chamber [44]. High load operating range of HCCI engine is limited by high combustion rate, resulting in high pressure rise rates, and heavy knocking as a result. Two main problems with such knocking are (i) unacceptable noise and (ii) accelerated wear on the mechanical components of the engine. The stricter criterion is combustion noise; therefore, a limit based on the combustion noise is appropriate for HCCI combustion. In this study, RI was used as measure of combustion noise.

Figure 12 shows variation of RI with λ and intake air temperature for gasoline and *n*-butanol. The figure shows the data for all tested engine operating conditions including the operating conditions in the knocking range. It can be observed from this figure that as mixture becomes richer, RI increases drastically at each intake air temperature for both fuels. When mixture becomes richer, combustion chamber temperature increases due to advanced combustion phasing, resulting in faster combustion rate, which leads to higher rate of pressure rise. Upon increasing the intake air temperature at any λ, RI increases. It can also be noticed from Fig. 12 that RI is more sensitive to λ for gasoline as compared to *n*-butanol for lower intake air temperature, because RI curves are relatively steeper for gasoline. The possible reason for this observation may be lower combustion efficiency of *n*-butanol, as observed earlier.

Maximum load, at which an engine can operate, depends on the maximum energy that can be injected into the combustion chamber. This therefore represents the lowest λ, at which, an engine can be operated. The richer λ limit depends on the accepted noise level. In this study, RI limit was chosen as 6 MW/m^2. Using this criterion, it can be seen that several data points are outside the range and combustion noise at these points is also very high. Combustion noise at any λ also depends on intake air temperature. Increased intake air temperature improves the combustion

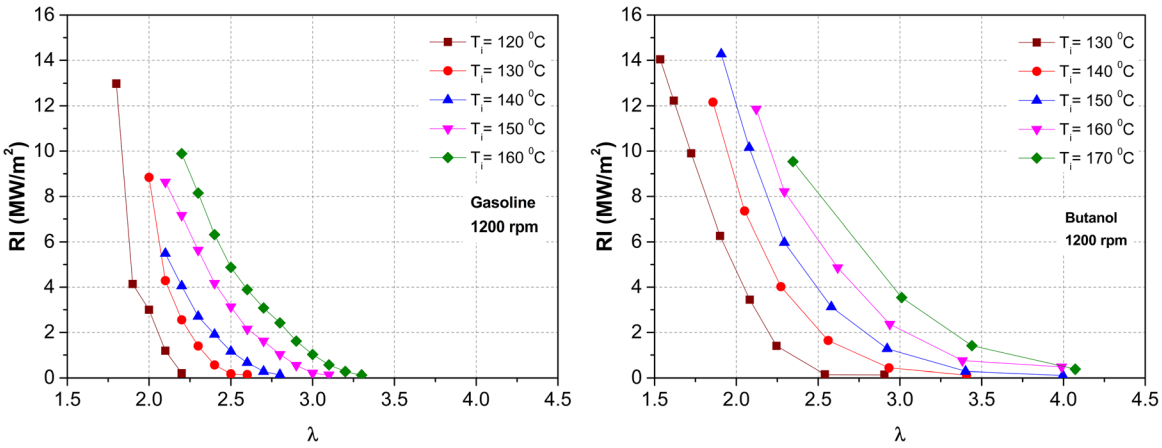

Fig. 12 Variation of RI with λ and T_i for gasoline and *n*-butanol HCCI

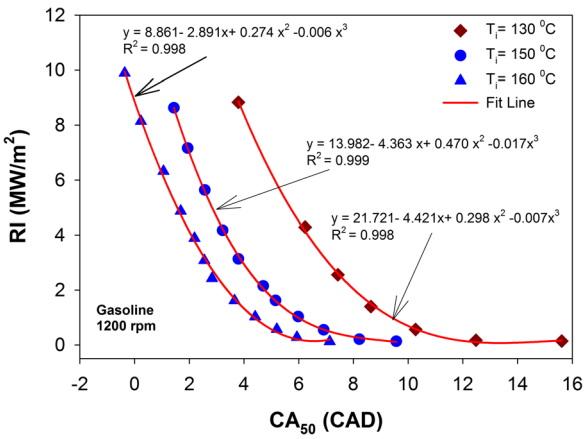

Fig. 13 Effect of combustion phasing on RI for gasoline HCCI

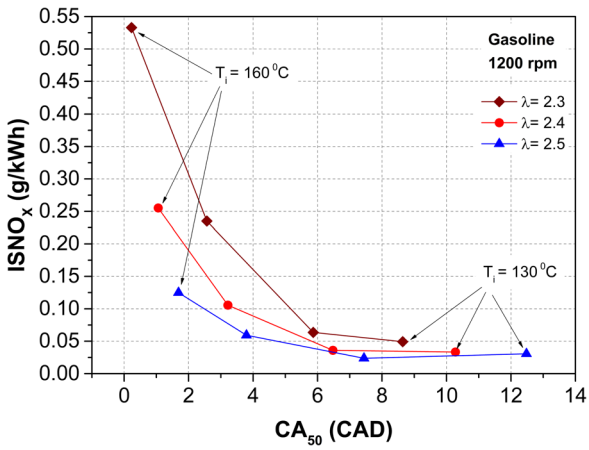

Fig. 14 Effect of combustion phasing (CA_{50}) on NO_x emissions for different λ for gasoline HCCI

efficiency. Therefore, these two factors act opposite to each other and optimum intake air temperature need to be selected for each λ.

Figure 13 shows the effect of combustion phasing (CA_{50}) on the RI at different intake air temperatures for gasoline at 1200 rpm. It can be noticed from this figure that RI increases as CA_{50} advances. Combustion phasing is therefore a major factor affecting the RI in HCCI combustion. The combustion phasing control is needed to retard CA_{50} and to reduce the RI at high RI operating conditions. Third order polynomial regression curve drawn through the experimental data points captures the trend in the behavior of RI. The RI according to CA_{50} could fit well into a polynomial equation, with a coefficient of determination (R^2) of over 0.99. Thus, RI can be estimated by CA_{50} at any intake air temperature.

3.6 Emission Characterization

3.6.1 NO_x Emissions. One of the major advantages in HCCI engine is its ultralow NO_x emission characteristics. Reduction in NO_x emissions can be explained by the combustion chamber temperature. NO_x formation is very sensitive to the peak combustion chamber temperature [33].

Figure 14 shows the effect of combustion phasing and intake air temperature on NO_x emissions at different λ using gasoline. It is observed that NO_x increases as combustion phasing advances at each λ. Increase in NO_x with advanced combustion phasing can be explained by higher combustion chamber temperature. Combustion chamber temperature increases with advanced combustion phasing due to early ignition and higher initial charge temperature results in higher NO_x formation. At combustion phasing after 6 CAD aTDC, formation of NO_x is very low (< 0.05 g/kW h).

Figure 15 shows the variation of NO_x emissions in HCCI operating range using gasoline and *n*-butanol, respectively, at 1200 rpm. The results show that HCCI combustion leads to massive reduction in NO_x emissions compared to conventional SI combustion. For example, typical NO_x emission in SI combustion is shown to be approximately 2500 ppm (11 g/kW h) at $\lambda = 1.1$, 1600 rpm, and $\eta_v = 50\%$ [33], while NO_x emissions are typically one order of magnitude lower in HCCI mode, and in some conditions, they are up to two orders of magnitude lower. NO_x emissions are highest for richer mixture closer to knock region and lowest for leaner mixture closer to misfire boundary for all fuels. This is due to higher in-cylinder combustion temperature prevailing for richer mixtures and lower in-cylinder temperature for leaner operating conditions.

It can be noticed from Fig. 15 that the maximum value of $ISNO_x$ from gasoline was 0.26 g/kW h and raw emissions of NO_x were 45 ppm. *n*-Butanol had even lower NO_x and the raw emission values were lower than 20 ppm in HCCI operating range. It can also be observed that the NO_x contour lines are inclined more toward horizontal, which suggests that λ contributed more to NO_x emissions as compared to intake air temperature in HCCI operating range for all fuels. NO_x emissions are therefore weakly sensitive to intake air temperature as compared to relative air–fuel ratio in HCCI operating range.

NO_x emissions from several conventional CI engines used in various previous studies are provided in Table 3. It can be seen

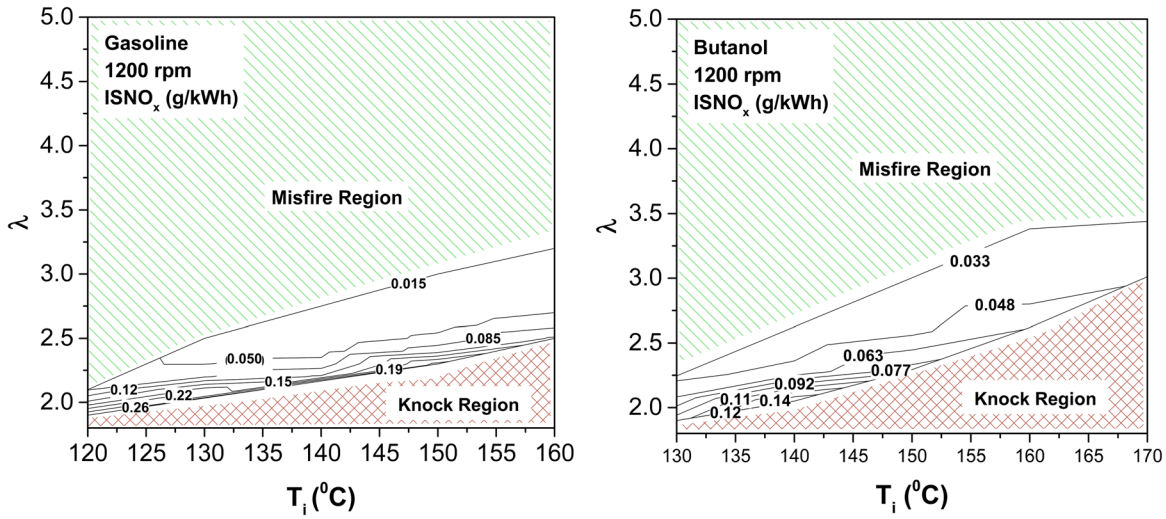

Fig. 15 NO_x emissions in HCCI operating range for gasoline and *n*-butanol

Table 3 Summary of typical conventional CI engine emission ranges

References	Engine	Speed (rpm)	NO_x (g/kW h)	HC (g/kW h)	CO (g/kW h)
[45]	CI	1800	7.5–10.0	0.02–0.50	1.0–15.0
[46]	CI	1900	4.5–8.0	0.2–2.0	0.5–7.0
[47]	CI	1800	6.0–7.5	0.7–2.7	0.7–3.8
[48]	CI	1800	5.0–10.0	0.5–5.0	1.0–12.0
[49]	CI	1800	5.0–7.5	0.1–8.0	1.0–13
[50]	CI	1800	5.0–10.0	0.8–9.0	1.0–15.0
[51]	CI	1500	7.0–12.0	0.1–0.5	4.0–15.0
[52]	CI	1500	10.0–14.0	0.5–1.0	3.0–10.0
[53]	CI	1200	5.0–12.5	0.1–0.5	1.0–30.0

from Table 3 that NO_x emissions from conventional CI engines are in the range of 4.5–14.0 g/kW h, depending on engine load and several other factors. Maximum $ISNO_x$ from this study among all the test conditions was lower than 0.3 g/kW h in HCCI operating range. Therefore, it can be summarized that NO_x emissions in HCCI operating mode are ultralow in comparison to conventional CI engines, which is also one of the main advantages of HCCI engine technology.

3.6.2 CO Emissions. The CO emissions are a result of incomplete oxidation/combustion of the fuel in the combustion chamber. CO emissions are strongly dependent on the combustion chamber temperature and higher temperatures are essential for homogeneous combustion of lean mixtures. At the end of combustion, the cylinder temperature becomes too low for complete oxidation; therefore, high CO formation takes place in HCCI engines.

Figure 16 shows the effect of IMEP and intake air temperature on CO formation at 1200 rpm for gasoline HCCI. It can be noticed that CO formation reduces drastically with increasing engine load for each intake air temperature. On increasing engine load, combustion chamber temperature increases due to higher fuel quantity burnt in order to produce higher IMEP at each intake air temperature. Thus, CO formation increases rapidly with lowering engine load and it is higher as compared to conventional engines. It can be noted that CO emission is very high (>15 g/kW h) for IMEP lower than 4 bar for gasoline, which further decreases drastically at IMEP higher than 4 bar (Fig. 16).

Figure 17 shows the variation of CO emissions for gasoline and *n*-butanol in HCCI operating range. It is observed that contours of CO lines are inclined, suggesting that CO is dependent on λ and intake air preheating. It is also observed that operating conditions

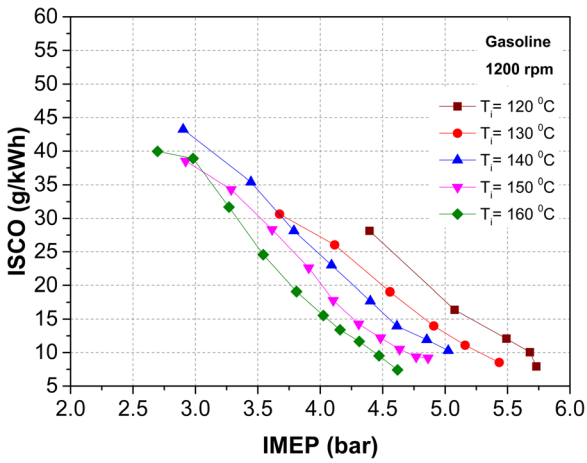

Fig. 16 Effect of IMEP and T_i on CO emissions from gasoline HCCI

close to the rich limit and knock limit result in early combustion phasing, which generates lower CO emissions for all test fuels. However, close to lean limit and misfire region, the resulting late combustion phasing generates very high CO for all fuels. Therefore, advanced combustion timings reduce the amount of CO produced, because the combustion temperature increases and there is more time available for reactions of in-cylinder oxidation of CO to take place. The maximum CO emission in HCCI operating range is as high as 39 g/kWh; however, it is rather simple to tackle CO emissions using standard exhaust gas after-treatment technologies. CO emissions from conventional CI engines used in various studies were summarized in Table 3. It can be noticed from Table 3 that CO emission from conventional CI engines was in the range of 0.5–15.0 g/kW h, depending on the engine load and a variety of other factors.

Indicated specific CO emissions from this study at 1200 rpm in HCCI operating range were in range of 5.0–39.0 g/kWh, depending on fuel and combustion timings. It can therefore be summarized that CO emission in HCCI engine are generally higher in comparison to conventional CI engines.

3.6.3 THC Emissions. Lower homogeneous in-cylinder temperature in HCCI engine reduces NO_x formation; however, the combustion temperature becomes too low to oxidize the fuel completely, resulting in higher unburned hydrocarbon emissions.

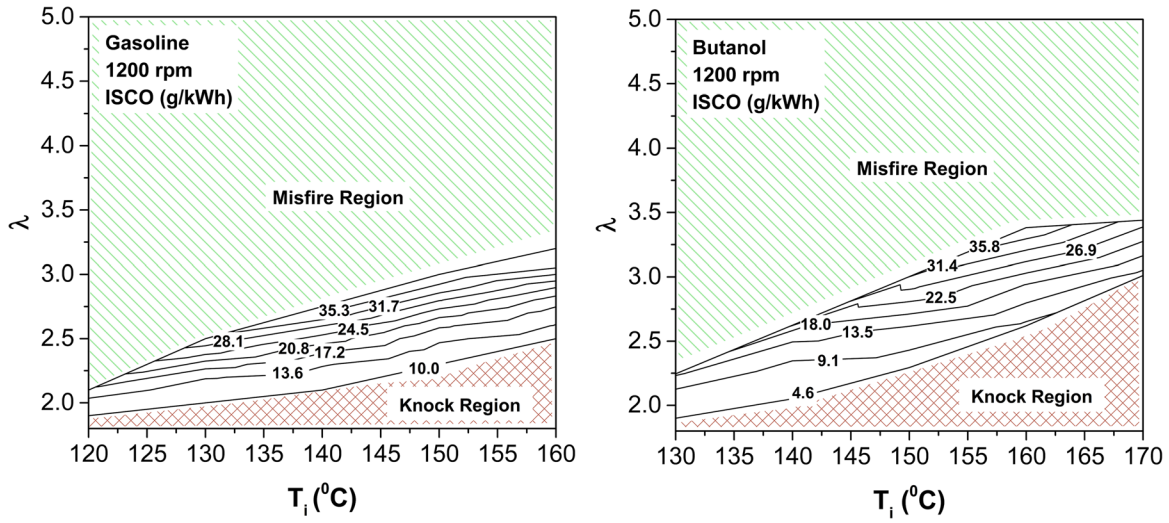

Fig. 17 Variation of CO emissions in HCCI operating range for gasoline and *n*-butanol

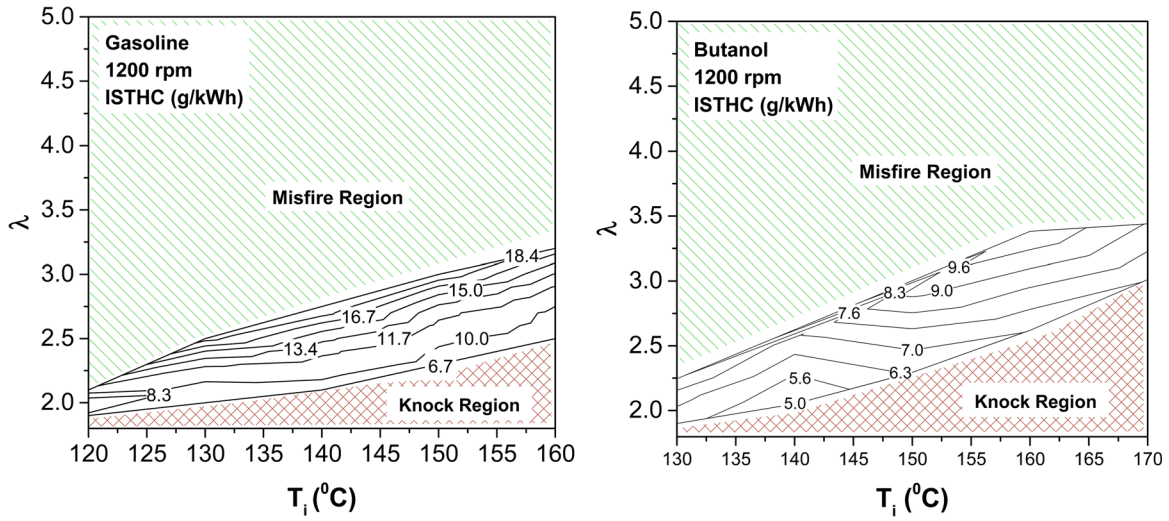

Fig. 18 Variation of THC emissions in HCCI operating range for gasoline and *n*-butanol

Combustion temperatures near the walls may be even lower due to significant heat losses. Combustion may therefore be quenched or may not occur at all, close to the cylinder walls. The main sources/mechanism of HC formation therefore includes crevice volumes, wall quenching, and bulk quenching.

Figure 18 shows the variation of THC emissions using gasoline and *n*-butanol in HCCI operating range at 1200 rpm. It is observed that contours of THC emission lines are inclined suggesting that THC emissions are dependent on λ and intake air preheating. In general, level of THC emissions from HCCI engines are higher over the entire operating range compared to typical CI combustion engines (Table 3). These emissions increase as λ is increased (i.e., leaner mixtures) for lower engine loads. This trend is seen because of lower heat release rate and lower combustion temperatures at lower engine loads. These conditions lead to lower oxidation rate of the fuel and incomplete combustion of some fuel/air mixtures during expansion and exhaust strokes.

It can also be noticed from Fig. 18 that mixture strength close to the rich limit and knocking zone results in early combustion phasing, which generates lower THC for all fuels. Combustion close to the lean limit and misfire region results in late combustion phasing, which generates high THC emissions for all fuels. Thus, advancing the combustion timing reduces the amount of THC produced, because these advanced combustion timings increase the combustion chamber temperature, which is conducive for higher in-cylinder oxidation of HC formed. Highest level of THC was 18.4 g/KW h and was obtained at the lowest engine loads for gasoline. This was one of main disadvantages of HCCI combustion engine; however, this can be tackled easily by catalytic conversion technology.

4 Conclusions

Experimental investigations were conducted on a modified HCCI engine operating at different intake air temperature and relative air fuel ratios using gasoline and *n*-butanol as fuel. It was found that IMEP was mainly affected by the air–fuel ratio in the HCCI operating region. HCCI operating region's area decreased with increasing engine speed for both fuels. Higher intake air temperature for auto-ignition was required at higher engine speeds for both fuels. HCCI operating range of *n*-butanol was slightly smaller than gasoline. Maximum IMEP found was 5.6 and 5.2 bar at 1200 rpm for gasoline and *n*-butanol, respectively. Main parameter affecting IMEP in the HCCI engine were fuel energy injected per cycle, P_{max} and CAP_{max}. Empirical correlation derived using these parameters showed good coefficient of determination and it

could predict the IMEP with a 0.3 bar uncertainty. Combustion efficiency in gasoline was found to be 96%; however, *n*-butanol showed lower combustion efficiency of 90%. *n*-Butanol showed lower indicated thermal efficiency and higher ISFC as compared to gasoline. It was found that as mixture became richer, RI increased drastically for both fuels. Third order polynomial regression curve captured the trends in behavior of RI at each intake air temperature with good coefficient of determination ($R^2 > 0.99$). HCCI combustion led to massive reduction in NO_x emissions compared to conventional combustion for all fuels. Maximum value of $ISNO_x$ from both fuels was 0.26 g/kW h and raw emissions of NO_x was 45 ppm in HCCI operating range. Emission of HC and CO was however found to be higher in HCCI mode as compared to conventional engines. In summary, *n*-butanol has good HCCI combustion characteristics and can be used as substitute of gasoline in HCCI engines.

Abbreviations

BDC = bottom dead center
CA = crank angle
CAD = crank angle degrees
CI = compression ignition
CO = carbon monoxide
COV = coefficient of variation
CA_{50} = crank angle position for 50% mass burn
EGR = exhaust gas recirculation
HC = unburned hydrocarbons
HCCI = homogeneous charge compression ignition engine
IMEP = indicated mean effective pressure
ISCO = indicated specific carbon monoxide
ISTHC = indicated specific total hydrocarbon
ISNOx = indicated specific nitrogen oxide
LabVIEW = laboratory virtual instrumentation engineering workbench
MBF = mass burn fraction
P = in-cylinder pressure
PM = particulate matter
Q = heat release
RI = ringing intensity
RIO = reconfigurable input-output
ROHR = rate of heat release
R^2 = coefficient of determination
SI = spark ignition
TDC = top dead center
T_i = inlet air temperature
V = volume of combustion chamber
W_{ind} = indicated work
γ = ratio of specific heats
η = efficiency
θ = crank angle position
λ = relative air-fuel ratio
σ = standard deviation

References

[1] Jin, C., Yao, M., Liu, H., Lee, C. F., and Ji, J., 2011, "Progress in the Production and Application of n-Butanol as a Biofuel," Renewable Sustainable Energy Rev., **15**(8), pp. 4080–4106.
[2] Hansen, A. C., Zhang, Q., and Lyne, P. W. L., 2005, "Ethanol–Diesel Fuel Blends–A Review," Bioresour. Technol., **96**(3), pp. 277–285.
[3] Hansen, A. C., Kyritsis, D. C., and Lee, C. F., 2009, "Characteristics of Biofuels and Renewable Fuel Standards," *Biomass to Biofuels–Strategies for Global Industries*, A. A. Vertes, H. P. Blaschek, H. Yukawa, and N. Qureshi, eds., Wiley, NY.
[4] Maurya, R. K., and Agarwal, A. K., 2011, "Experimental Study of Combustion and Emission Characteristics of Ethanol Fuelled Port Injected Homogeneous Charge Compression Ignition (HCCI) Combustion Engine," Appl. Energy, **88**(4), pp. 1169–1180.
[5] Fortman, J. L., Chhabra, S., Mukhopadhyay, A., Chou, H., Lee, T. S., Steen, E., and Keasling, J. D., 2008, "Biofuel Alternatives to Ethanol: Pumping the Microbial Well," Trends Biotechnol., **26**(7), pp. 375–381.
[6] Ezejia, T. C., Qureshib, N., and Blascheka, H. P., 2005, "Continuous Butanol Fermentation and Feed Starch Retrogradation: Butanol Fermentation Sustainability Using Clostridium Beijerinckii BA101," J. Biotechnol., **115**(2), pp. 179–187.
[7] Maurya, R. K., and Agarwal, A. K., 2009, "Experimental Investigation of the Effect of the Intake Air Temperature and Mixture Quality on the Combustion of a Methanol and Gasoline Fuelled Homogeneous Charge Compression Ignition Engine," Proc. Inst. Mech. Eng., Part D, **223**(11), pp. 1445–1458.
[8] Aceves, S. M., Martinez-Frias, J., and Reistad, G. M., 2006, "Analysis of Homogeneous Charge Compression Ignition (HCCI) Engines for Cogeneration Applications," ASME J. Energy Resour. Technol., **128**(1), pp. 16–27.
[9] Maurya, R. K., and Agarwal, A. K., 2012, "Statistical Analysis of Cyclic Variation of Heat Release Parameters in HCCI Combustion of Methanol and Gasoline Fuel," Appl. Energy, **89**(1), pp. 228–236.
[10] Li, H., Neill, W. S., and Chippior, W. L., 2012, "An Experimental Investigation of HCCI Combustion Stability Using n-Heptane," ASME J. Energy Resour. Technol., **134**(2), p. 022204.
[11] Soloiu, V., Duggan, M., Ochieng, H., Williams, D., Molina, G., and Vlcek, B., 2013, "Investigation of Low Temperature Combustion Regimes of Biodiesel With n-Butanol Injected in the Intake Manifold of a Compression Ignition Engine," ASME J. Energy Resour. Technol., **135**(4), p. 041101.
[12] El-Din, H., Elkelawy, M., and Yu-Sheng, Z., 2010, "HCCI Engines Combustion of CNG Fuel With DME and H2 Additives," SAE Technical Paper No. 2010-01-1473.
[13] Jang, J., Yang, K., and Bae, C., 2009, "The Effect of Injection Location of DME and LPG in a Dual Fuel HCCI Engine," SAE Technical Paper No. 2009-01-1847.
[14] Maurya, R. K., and Agarwal, A. K., 2011, "Experimental Investigations of Gasoline HCCI Engine During Startup and Transients," SAE Technical Paper No. 2011-01-2445.
[15] Yan, Y., Yu-Sheng, Z., Yong-Tian, C., Zu-Di, C., and Ge, X., 2010, "Study on HCCI Combustion and Emission Characteristics of Diesel Engine Fueled With Methanol/DME," SAE Technical Paper No. 2010-01-0578.
[16] Gérard, D., Besson, M., Hardy, J., Croguennec, S., Thomine, M., Aoyama, S., and Tomita, M., 2008, "HCCI Combustion on a Diesel VCR Engine," SAE Technical Paper No. 2008-01-1187.
[17] Lu, X., Han, D., and Huang, Z., 2011, "Fuel Design and Management for the Control of Advanced Compression-Ignition Combustion Modes," Prog. Energy Combust. Sci., **37**(6), pp. 741–783.
[18] Regalbuto, C., Pennisi, M., Wigg, B., and Kyritsis, D., 2012, "Experimental Investigation of Butanol Isomer Combustion in Spark Ignition Engines," SAE Technical Paper No. 2012-01-1271.
[19] Wigg, B., Coverdill, R., Lee, C., and Kyritsis, D., 2011, "Emissions Characteristics of Neat Butanol Fuel Using a Port Fuel-Injected, Spark-Ignition Engine," SAE Technical Paper No. 2011-01-0902.
[20] Szwaja, S., and Naber, J. D., 2010, "Combustion of n-Butanol in a Spark-Ignition IC Engine," Fuel, **89**(7), pp. 1573–1582.
[21] Yang, J., Wang, Y., and Feng, R., 2011, "The Performance Analysis of an Engine Fueled With Butanol-Gasoline Blend," SAE Technical Paper No. 2011-01-1191.
[22] Yang, J., Yang, X., Liu, J., Han, Z., and Zhong, Z., 2009, "Dyno Test Investigations of Gasoline Engine Fueled With Butanol-Gasoline Blends," SAE Technical Paper No. 2009-01-1891.
[23] Chen, G., Yu, W., Li, Q., and Huang, Z., 2012, "Effects of n-Butanol Addition on the Performance and Emissions of a Turbocharged Common-Rail Diesel Engine," SAE Technical Paper No. 2012-01-0852.
[24] Miers, S., Carlson, R., McConnell, S., Ng, H., Wallner, T., and Esper, J., 2008, "Drive Cycle Analysis of Butanol/Diesel Blends in a Light-Duty Vehicle," SAE Technical Paper No. 2008-01-2381.
[25] Zoldy, M., Hollo, A., and Thernesz, A., 2010, "Butanol as a Diesel Extender Option for Internal Combustion Engines," SAE Technical Paper No. 2010-01-0481.
[26] Yamamoto, S., Agui, Y., Kawaharada, N., Ueki, H., Sakaguchi, D., and Ishida, M., 2012, "Comparison of Diesel Combustion Between Ethanol and Butanol Blended With Gas Oil," SAE Technical Paper No. 2012-32-0020.
[27] Gu, X. L., Huang, Z. H., Cai, J., Gong, J., Wu, X. S., and Lee, C. F., 2012, "Emission Characteristics of a Spark-Ignition Engine Fuelled With Gasoline-n-Butanol Blends in Combination With EGR," Fuel, **93**, pp. 611–617.
[28] Chotwichien, A., Luengnaruemitchai, A., and Jai-In, S., 2009, "Utilization of Palm Oil Alkyl Esters as an Additive in Ethanol-Diesel and Butanol-Diesel Blends," Fuel, **88**(9), pp. 1618–1624.
[29] Liu, H. F., Lee, C. F., Huo, M., and Yao, M. F., 2011, "Combustion Characteristics and Soot Distributions of Neat Butanol and Neat Soybean Biodiesel," Energy Fuels, **25**(7), pp. 3192–3203.
[30] Zhang, Q., Yao, M., Zheng, Z., Liu, H., and Xu, J., 2012, "Experimental Study of n-Butanol Addition on Performance and Emissions With Diesel Low Temperature Combustion," Energy, **47**(1), pp. 515–521.
[31] Maurya, R. K., and Agarwal, A. K., 2013, "Digital Signal Processing of Cylinder Pressure Data for Combustion Diagnostics of HCCI Engine," Mech. Syst. Signal Process., **13**(1), pp. 95–109.
[32] Maurya, R. K., and Agarwal, A. K., 2013, "Investigations on the Effect of Measurement Errors on Estimated Combustion and Performance Parameters in HCCI Combustion Engine," Measurement, **46**(1), pp. 80–88.
[33] Heywood, J. B., 1988, *Internal Combustion Engine Fundamentals*, McGraw Hill, NY.
[34] Gatowski, J. A., Balles, E. N., Chun, K. M., Nelson, F. E., Ekchian, J. A., and Heywood, F. B., 1984, "A Heat Release Analysis of Engine Pressure Data," SAE Technical Paper No. 841359.

[35] Soyhan, H. S., Yasar, H., Walmsley, H., Head, B., Kalghatgi, G. T., and Sorusbay, C., 2009, "Evaluation of Heat Transfer Correlations for HCCI Engine Modelling," Appl. Therm. Eng., **29**(2–3), pp. 541–549.
[36] Eng, J., 2002, "Characterization of Pressure Waves in HCCI Combustion," SAE Technical Paper No. 2002-01-2859.
[37] Christensen, M., Hultqvist, A., and Johansson, B., 1999, "Demonstrating the Multi Fuel Capability of a Homogeneous Charge Compression Ignition Engine With Variable Compression Ratio," SAE Technical Paper No. 1999-01-3679.
[38] Iida, N., 2007, "Natural Gas HCCI Engines," in *HCCI and CAI Engines for the Automotive Industry*, H. Zhao, ed., Woodhead Publishing Limited, Cambridge, UK.
[39] Johansson, T., Borgqvist, P., Johansson, B., Tunestal, P., and Aulin, H., 2010, "HCCI Heat Release Data for Combustion Simulation, Based on Results From a Turbocharged Multi Cylinder Engine," SAE Technical Paper No. 2010-01-1490.
[40] Johansson, T., Johansson, B., Tunestål, P., and Aulin, H., 2009, "HCCI Operating Range in a Turbo-Charged Multi Cylinder Engine With VVT and Spray-Guided DI," SAE Technical Paper No. 2009-01-0494.
[41] Shahbakhti, M., Ghazimirsaied, A., and Koch, C. R., 2010, "Experimental Study of Exhaust Temperature Variation in a Homogeneous Charge Compression Ignition Engine," Proc. Inst. Mech. Eng., Part D, **224**, pp. 1177–1197.
[42] Christensen, M., Johansson, B., and Einewall, P., 1997, "Homogeneous Charge Compression Ignition (HCCI) Using Isooctane, Ethanol and Natural Gas - A Comparison With Spark Ignition Operation," SAE Technical Paper No. 972874.
[43] Christensen, M., and Johansson, B., 1999, "Homogeneous Charge Compression Ignition With Water Injection," SAE Technical Paper No. 1999-01-0182.
[44] Yeom, K., and Bae, C., 2009, "Knock Characteristics in Liquefied Petroleum Gas (LPG)-Dimethyl Ether (DME) and Gasoline-DME Homogeneous Charge Compression Ignition Engines," Energy Fuels, **23**(4), pp. 1956–1964.
[45] Agarwal, A. K., and Dhar, A., 2010, "Comparative Performance, Emission, and Combustion Characteristics of Rice-Bran Oil and Its Biodiesel in a Transportation Diesel Engine," ASME J. Eng. Gas Turbines Power, **132**(6), p. 064503.
[46] Shi, X., Yu, Y., He, H., Shuai, S., Wang, J., and Li, R., 2005, "Emission Characteristics Using Methyl Soyate–Ethanol–Diesel Fuel Blends on a Diesel Engine," Fuel, **84**(9), pp. 1543–1549.
[47] Shi, X., Pang, X., Mu, Y., He, H., Shuai, S., Wang, J., Chen, H., and Li, R., 2006, "Emission Reduction Potential of Using Ethanol–Biodiesel–Diesel Fuel Blend on a Heavy-Duty Diesel Engine," Atmos. Environ., **40**(14), pp. 2567–2574.
[48] Di, Y., Cheung, C. S., and Huang, Z., 2009, "Comparison of the Effect of Biodiesel-Diesel and Ethanol-Diesel on the Gaseous Emission of a Direct-Injection Diesel Engine," Atmos. Environ., **43**(17), pp. 2721–2730.
[49] Zhang, Z. H., Cheung, C. S., Chan, T. L., and Yao, C. D., 2009, "Emission Reduction From Diesel Engine Using Fumigation Methanol and Diesel Oxidation Catalyst," Sci. Total Environ., **407**(15), pp. 4497–4505.
[50] Zhua, L., Cheung, C. S., Zhang, W. G., and Huang, Z., 2011, "Combustion, Performance and Emission Characteristics of a DI Diesel Engine Fueled With Ethanol Biodiesel Blends," Fuel, **90**(5), pp. 1743–1750.
[51] Mani, M., Subash, C., and Nagarajan, G., 2009, "Performance, Emission and Combustion Characteristics of a DI Diesel Engine Using Waste Plastic Oil," Appl. Therm. Eng., **29**(13), pp. 2738–2744.
[52] Geo, V. E., Nagarajan, G., and Nagalingam, B., 2010, "Studies on Improving the Performance of Rubber Seed Oil Fuel for Diesel Engine With DEE Port Injection," Fuel, **89**(11), pp. 3559–3567.
[53] Yoon, S. H., and Lee, C. S., 2011, "Effect of Biofuels Combustion on the Nanoparticle and Emission Characteristics of a Common-Rail DI Diesel Engine," Fuel, **90**(10), pp. 3071–3077.